Available online at www.sciencedirect.com
SCIENCE DIRECT®
Journal of volcanology and geothermal research
ELSEVIER
Journal of Volcanology and Geothermal Research 129 (2004) 109–123
www.elsevier.com/locate/jvolgeores

Magma fragmentation speed: an experimental determination

O. Spieler *, D.B. Dingwell, M. Alidibirov

Earth and Environmental Sciences, University of Munich, Theresienstr. 41/III, 80333 Munich, Germany

Received 9 October 2002; received in revised form 20 January 2003; accepted 25 February 2003

Abstract

The propagation speed of a fragmentation front, combined with the ascent velocity of magma is, in all likelihood, a controlling factor in the dynamics of explosive volcanic eruptions. Direct measurement of the 'fragmentation speed' in natural systems appears to be impossible at present. Fortunately, laboratory experiments can provide information on the propagation speed of the fragmentation front. Here we present the results of fragmentation speed determinations using a so-called 'fragmentation bomb'. These are, to the best of our knowledge, the first in situ fragmentation speed determinations performed on magma. Natural magma samples (Merapi basaltic andesite, Mount St. Helens dacite and Unzen dacite) have been investigated in the temperature range of 20–950°C and at pressures up to 25 MPa. Two techniques have been employed. Firstly, in experiments at 20°C, dynamic pressure transducers were placed above and below the magma samples and the fragmentation speed of the magma sample was derived from an analysis of the decompression curves. Secondly, at elevated temperatures, an alternative technique was introduced and successfully employed. This involved the severing via fragmentation of conducting wires placed within the samples at various heights. Fragmentation speeds are very low, falling in the range of 2–70 m/s and increasing with an increase in the magnitude of the decompression step responsible for the fragmentation. The first high-temperature determination seems consistent with low-temperature results. Implications for explosive volcanism are discussed briefly.

Keywords: fragmentation; decompression; explosive; eruption; experiments; dynamic

1. Introduction

Explosive volcanism is capable of generating an array of eruptive phenomena that range from Plinian eruption columns to pyroclastic flows. The fragmentation of magma is the defining feature of this explosive volcanism. It should come then as no surprise that during the past three decades processes controlling explosive eruption have been widely debated and that the nature of fragmentation has played a central role in that debate (McBirney and Murase, 1970; Sparks, 1978; Wohletz and McQueen, 1984; Heiken and Wohletz, 1991; Sato et al., 1992; Fink and Kieffer, 1993; Proussevitch et al., 1993; Alidibirov, 1994; Cashman and Mangan, 1994; Hurwitz and Navon, 1994; Sparks et al., 1994; Thomas et al., 1994; Barclay et al., 1995; Sugioka and Bursik, 1995; Zimanowski et al., 1997; Proussevitch and Sahagian, 1998; Kaminski and Jaupart, 1998; Dingwell, 1998a,b; Papale, 1999; Zhang, 1999; Martel et al., 2000; Melnik, 2000; Alidibi-

* Corresponding author.

0377-0273/03/$ – see front matter © 2003 Elsevier B.V. All rights reserved.
doi:10.1016/S0377-0273(03)00235-X

rov and Dingwell, 2000; Martel et al., 2001; Spieler et al., 2003).

It has also become clear in recent years that a relatively efficient fragmentation of magma can be generated by a variety of physical and chemical mechanisms (phase transitions etc.) in magmatic conduits and domes. Magma fragmented in explosive eruptions is present in erupted products in a wide range of crystallinity and vesicularity. The inferred ranges of values of physico–chemical properties, such as viscosity, are also relatively wide. Further, the range of pressures (from one to hundreds of MPa) and temperatures (over 1000°C) over which fragmentation appears possible is considerable. As a result of these observations and inferences, it has become clear that a model to describe magma fragmentation must be able to cope with significant ranges in fragmentation conditions and fragmenting materials.

The timing, speed and efficiency of magma fragmentation are almost certainly the factors controlling the nature of the fragmentation products and thus also a significant influence on the flows they produce. As such, it becomes an important experimental goal to determine those parameters in systems where sufficient attention is paid to the physico–chemical characterisation of the magma and the conditions of fragmentation.

During the last decade a number of laboratory simulations have contributed to the debate on the mechanism and efficiency of magmatic fragmentation performed using synthetic analogues (Hill and Sturtevant, 1990; Sparks et al., 1994; Mader et al., 1994, 1996; Sugioka and Bursik, 1995; Phillips et al., 1995; Zhang et al., 1997, Ichihara et al., 2002). Experiments on analogue materials bring with them a number of experimental and theoretical advantages in the investigation of magma fragmentation. They are, and will undoubtedly remain, a key experimental component in the search for a mechanistically-based and fully quantifiable model of magma fragmentation. Alidibirov and Dingwell (1996a,b) emphasised that a further aspect of fragmentation, namely the role of magma properties and physical state in controlling fragmentation, should be experimentally accessible. This they achieved by adapting the high-pressure high-temperature methods of experimental petrology to the investigation of natural magma samples. They developed the fragmentation bomb, the facility employed in this study.

The experimental results presented here represent the first successful determination of the fragmentation speed of magma at high temperature. The speeds obtained have implications for the propagation of fragmentation fronts in erupting magma columns and the efficiency of the generation of new surfaces in the form of pyroclast production.

2. Experimental apparatus and methods

The present experiments were performed using a modified version of the fragmentation bomb, a shock tube apparatus introduced to experimental volcanology by Alidibirov and Dingwell (1996a,b). The reader is referred to Alidibirov and Dingwell (1996b) for an extensive description of the original device. Briefly, the method involves the rapid decompression of cylindrical samples of natural magma (50 mm length and 17 mm diameter, respectively) at variable temperatures and pressures. The fragmentation bomb consists of two major sections (Fig. 1). A high-pressure, high-temperature autoclave (HPT) and a large-volume low-pressure tank (LPT). These two sections are separated by a set of specially designed rupture diaphragms whose task is to fail at a certain value of pressure difference (ΔP) or 'overpressure' between the HPT and the LPT. The decompression of the sample is thus controlled by the rapid opening of the diaphragms at a selected overpressure.

Important modifications to this experimental facility have been made here. These include: (1) the reconfiguration of the gas supply system to minimise noise-like signal reflection at the rim of the open diaphragm; (2) a newly constructed stainless steel LPT with a volume of 0.38 m^3 and a length of 3 m for enhanced particle recovery and prevention of secondary fragmentation; and (3) the addition of a triple-diaphragm-based trigger-system. This last modification has yielded a high precision for the fragmentation pressure, even at temperatures up to 900°C. The first dia-

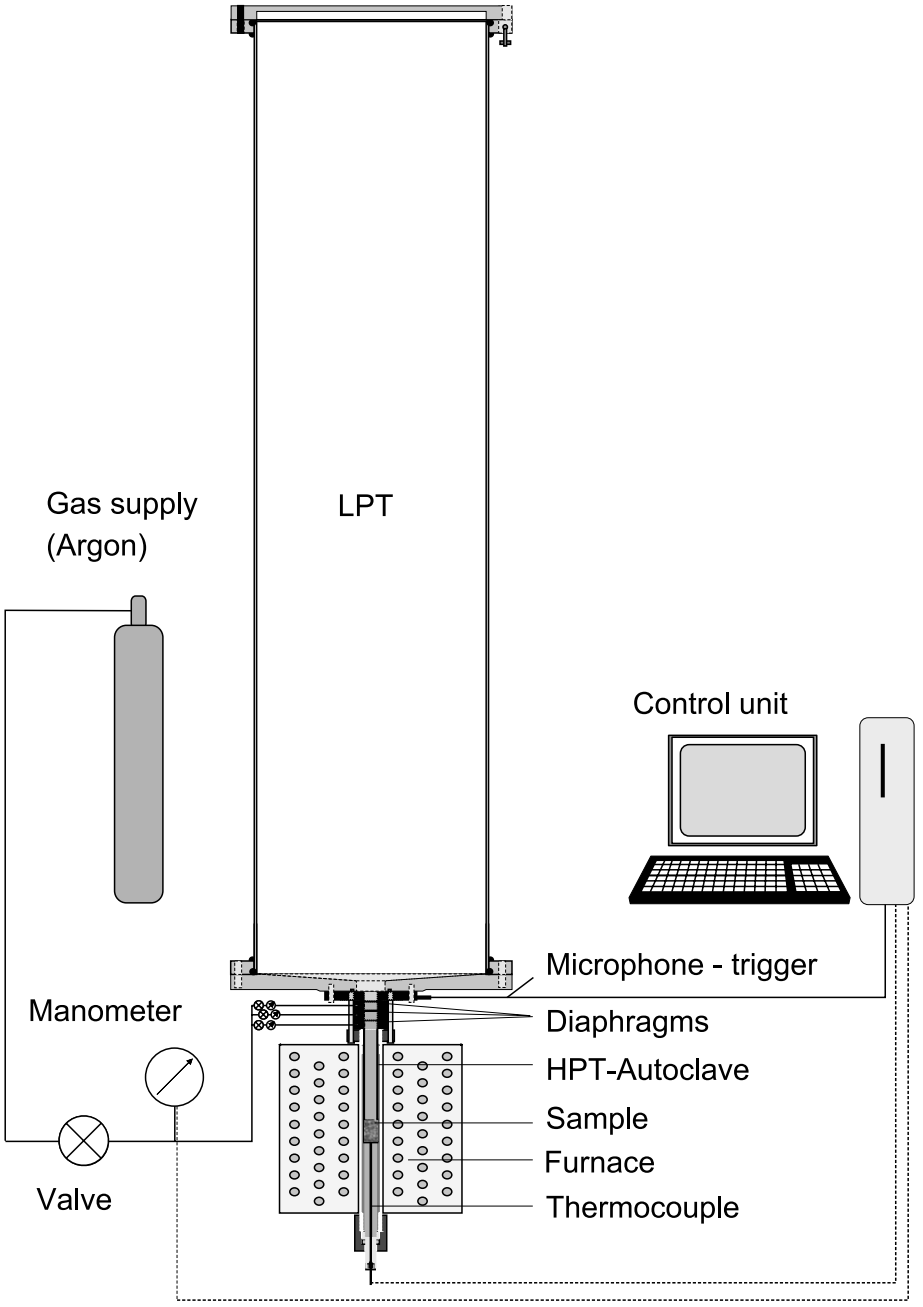

Fig. 1. Schematic illustration of the essential components of the modified fragmentation bomb (Alidibirov and Dingwell, 1996a,b). The apparatus consists of a 3-m-long stainless steel LPT with 40 cm inner diameter and a cold seal autoclave, both separated by a set of diaphragms. Argon is supplied through capillary tubing. A computer is used as control unit. For a detailed description of the initial design, see Alidibirov and Dingwell (1996b). The modifications presented here include a stainless steel LPT and a new gas-trigger system (see text).

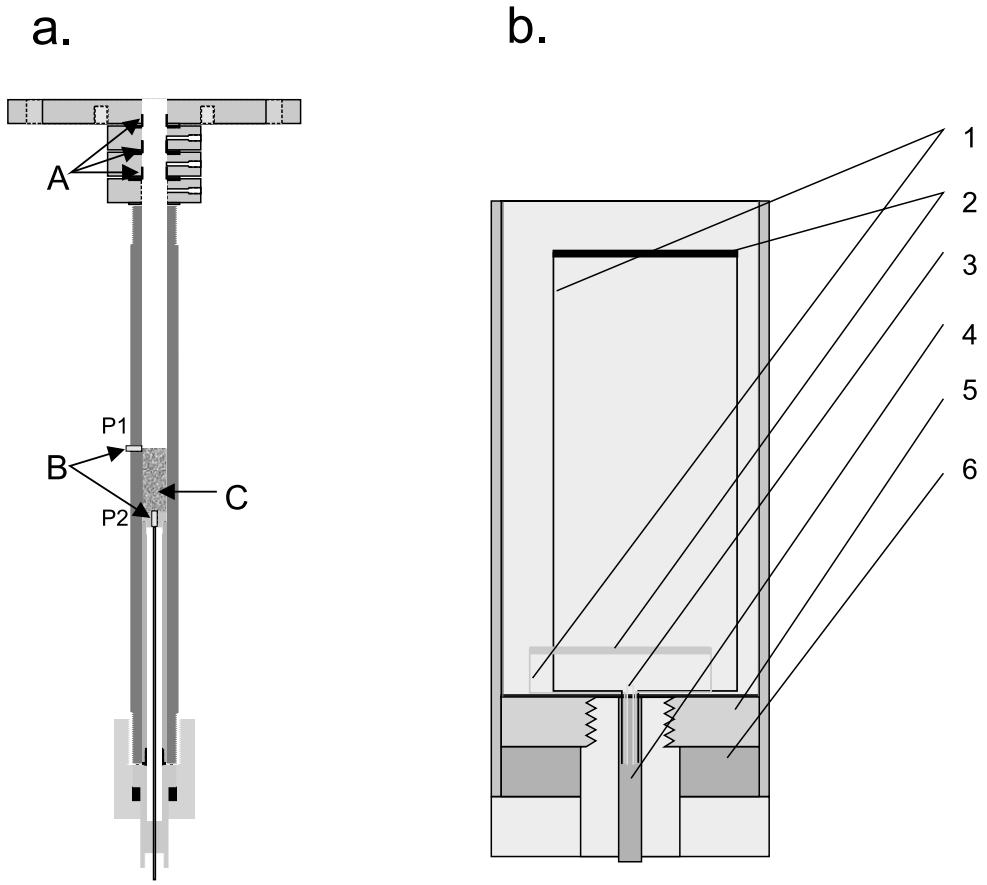

Fig. 2. (a) The experimental configuration of the autoclave used for the determination of fragmentation speed at low temperatures (max. 340°C). The speed is determined by comparing decompression signals between two dynamic pressure transducers. Key: A, open diaphragms; B, dynamic pressure transducer (PCB 113A21). P1 is the pressure transducer at the upper free surface of the sample. P2 is located 0.1 mm below the base of the sample. C, sample glued gas-tight in a sample tube (length 50 mm, diameter 17 mm). The thermocouple for room temperature experiments is placed outside the autoclave since the recording is not fast enough to analyse temperature changes during the fragmentation. (b) The experimental configuration of the sample holder used for the determination of fragmentation speed at high temperatures (max. 950°C). The speed is determined by the separation distance between the graphite rods and time interval of the signal cut off. Key: 1, platinum wire; 2, graphite rod; 3, thermocouple; 4, Al_2O_3 6-bore tubing; 5, stainless steel plate for heat conduction; 6, alumina plate as thermal insulation.

phragm above the HPT is stabilised by the elevated pressure in the next, adjacent chamber. The pressure difference between the first chamber and the autoclave is held below 50% of the diaphragm rupture pressure and is used primarily as a thermal shield for the second diaphragm. The decompression is triggered by overpressurisation of the upper diaphragm. Using this method it is possible to trigger precisely the decompression of the autoclave, even at pressures above 20 MPa (less than 1% pressure error). This gas trigger was originally invented for the high-temperature experiments to permit longer dwell times of our samples.

The pressure histories of low-temperature experiments were obtained using a steel high-pressure section (20 mm inner diameter, 450 mm in length) equipped with two dynamic piezoelectric pressure transducers (PCB Piezotronics Inc., E113A21), each with a response time of 1 μs. One transducer (P1) was installed in a bore with a connection orifice (1 mm length, 1 mm diame-

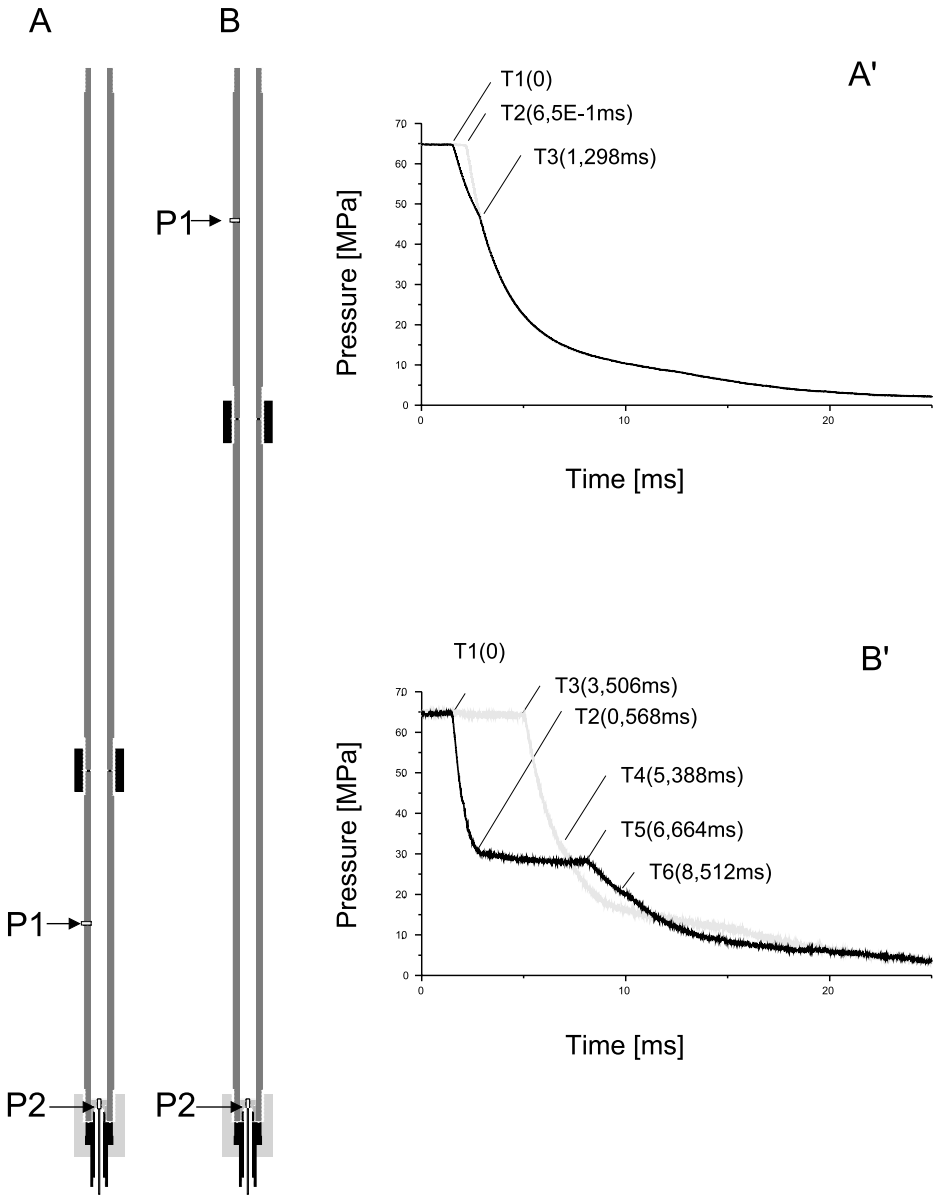

Fig. 3. Calibration of the system included the determination of the RW speed in two elongated configurations of the empty autoclave (A, B) which minimises errors and potential signal reflections. Key: P1, upper pressure transducer; P2, lower pressure transducer. The configuration of the calibration experiments is given on the left side. The recorded decompression data for the experiments is provided on the right (the black and grey lines correspond to P1 and P2, respectively).

ter) at the height of the upper sample surface, 212 mm below the lower diaphragm (Fig. 2). The second transducer (P2) was screwed into the bottom of a gas-tight fitting sample container (Fig. 2). Samples were installed inside tube-like brass containers using a thermal curing glue (Crystalbond 509, T-E Klebetechnik, Germany) to provide good adhesion of the sample and prevent significant amounts of gas from residing between the samples and the container wall.

The fragmentation speed measurements at high temperatures necessitated a further new experi-

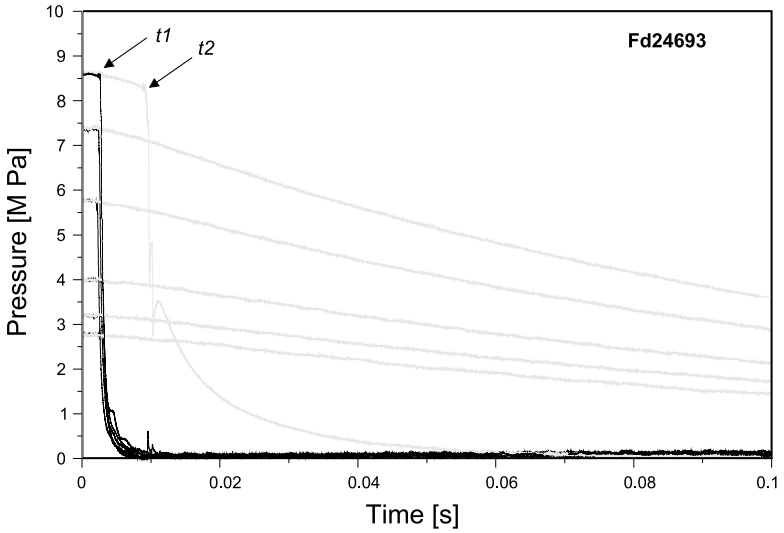

Fig. 4. Pressure history of six experiments on FD24693, an Unzen dacite with 16.4 vol% open porosity. Each experiment is represented by a pair of recorded pressure signatures (the black and grey lines correspond to P1 and P2, respectively). In the first four experiments (at 2.8, 3.2, 4, and 7.4 MPa) no fragmentation occurred and the pressure history below the sample shows a slow permeability controlled depressurisation. In a fifth experiment, performed on a sample after the 7.4 MPa applying a reduced pressure of 5.7 MPa, a potential permeability change due to rapid filtration flow was not observed. In the sixth experiment (at 8.6 MPa) fragmentation occurred. The time interval between $t1$ (arrival of the rarefaction front at P1) and $t2$ (rapid pressure drop at P2 below the sample) is used to calculate T_{fr}, the duration of the sample disintegration.

mental design. A Nimonic® 105 externally heated autoclave with an internal diameter of 28 mm was constructed. Using a 28/1-mm steel tube as sample holder the diameter of the sample is 26 mm. The length of the sample cylinder was extended to 60 mm giving a larger (2.8×) sample volume. A high-temperature cement (WH-Feuerfestkitt 1500, W. Haldenwanger, Berlin, Germany) is used to connect the sample with the steel tube and the bottom plate. By adding a 5-mm Alsint disc under the stainless steel bottom plate we were able to improve the temperature gradient and reduced the temperature drop through the sample to less than 12°C at 900°C. To minimise the excess gas volume below the sample, the inner diameter of the autoclave was reduced to 10 mm under the sample. The gas supply system and the diaphragms had to be adapted to the new requirements. Fig. 2b is a schematic illustration of the high-temperature experiment. Drill holes perpendicular to the long axis of the sample cylinder were used to place graphite rods as electrical conductors with known distance in the path of the fragmentation. We used 0.3-mm graphite (pencil lead) in the first set of experiments since a fast fragmentation of the conductor was neccessary. A 5V (DC) current applied to the graphite rods is monitored as computer signal. The experiment was designed such that the fragmentation front would break the upper graphite rod causing a signal drop followed by a second signal drop due the fragmentation of the second graphite rod. The time between the two signal drops, combined with the known separation distance of the bores thus yields the speed of the fragmentation front. It should be noted that in one early experiment we obtained a speed of ~3500 m/s, approximately the speed of sound in the solid matrix of the foam. Clearly, in this case the unloading wave that coupled into the sample was strong enough to fracture the 0.3-mm graphite rod. A Pt/$Pt_{90}Rh_{10}$ (Type S) thermocouple was placed at a depth of 1 mm in the bottom of the sample to record the experimental run temperature.

The high-pressure section of the fragmentation bomb is slowly pressurised by argon, used as a pressure medium. The gas, supplied through a capillary at the top of the HPT, fills the free space

of the autoclave between the sample and the diaphragm (distance = 212 mm) and infiltrates the open pores of the sample. At a pre-selected pressure the upper adjacent chambers are over-pressurised. This acts to generate a rupture of the diaphragm causing the propagation of a shock wave into the LPT. Quasi-instantaneously the lower diaphragm opens and a rarefaction wave (RW) is established (whose speed has been determined in this study at 328–344 m/s) travelling into the HPT. Fig. 3 illustrates the calibration of signal reflections in the fragmentation bomb. The resulting speed of the RW, measured in different configurations, was needed to locate possible signal reflections. Fig. 3A,B shows experiments to calculate the velocity of the RW. The distance of the pressure transducers (P1 and P2) in case A is 220 mm with a recorded travel time of 0.65 ms (T2 in A′) leading to a velocity of 339 m/s. In case B the distance between the transducers is 1150 mm and the recorded travel time corresponds to 3.506 ms (T3 in B′) giving a velocity of 328 m/s. A pressure plateau is established at T2 (B′ at 0.568 ms) and persists until the reflected RW passes P1 at T5 (6.664 ms in B′). This plateau is followed by a lower plateau on the records of the lower transducer and is a reminder that ΔP on top of the sample is not identical to the initial pressure in the autoclave. The small peaks at T4 and T6, respectively, correspond to signal reflections at the rim of the open diaphragms.

Upon reaching the sample surface the RW couples into the sample, resulting in a P-wave that travels through the sample and simultaneously generates the rapid decompression of the sample. The depressurisation of the sample surface is a function of: (1) the initial pressure difference between the HPT and LPT, (2) the temperature, and (3) the geometry (diameter) of the autoclave. If the decompression exceeds the fragmentation threshold of the sample, a fragmentation wave is generated which successively fragments the sample in planes perpendicular to the axis of decompression. The progression of the fragmentation wave is recorded as function of pressure and time below the sample.

3. Investigated samples

The materials investigated in the present study are: (1) three samples of low porous dacite from

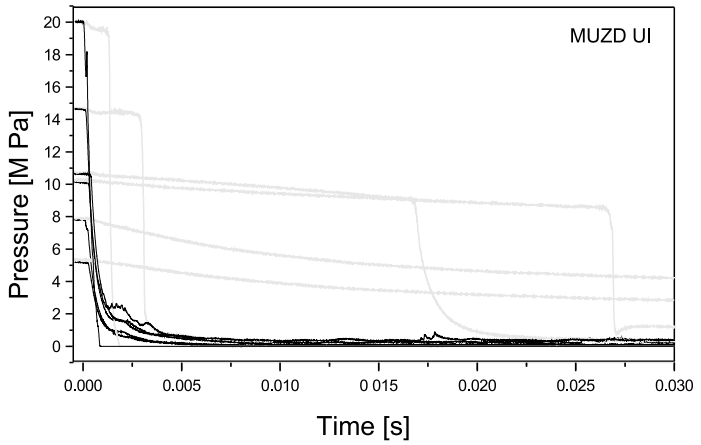

Fig. 5. Pressure curves of decompression experiments on the second sample of Unzen dacite with 21.5 vol% porosity (MUZD UI). Decompression of 10.3 MPa yields a fragmentation speed of ~2.1 m/s; decompression of 10.8 MPa yields a higher fragmentation speed of 3.0 m/s. Further increase in the decompression to 14.6 MPa increases the speed to 18 m/s. The final test (at 20 MPa) yielded a speed of 38.9 m/s. The signal of the upper pressure transducer (black) includes a reflection of the RW at 1.2–2.4 ms. The signal noise recorded (in most experiments) before the pressure drop below the sample reflects the passage of large individual particles between the sample and the transducer. The experiments at 4.8 and 7.8 MPa were below ΔP_{fr} and did not fragment.

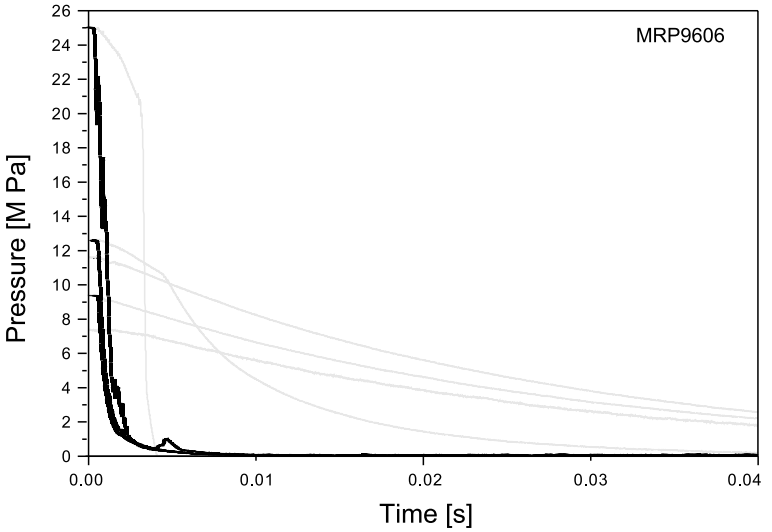

Fig. 6. Results of five dynamic fragmentation tests on Merapi andesite (MRP 9606). The experiments below 11.5 MPa show no fragmentation and the pressure below the sample (grey line) is reduced by filtration flow through the sample. At 11.5 MPa 1 mm of the sample was removed. The pressure below the sample follows the same decompression path as in the experiments at lower initial pressure. At the threshold pressure of 12.5 MPa the lower pressure transducer records a sudden pressure drop corresponding to a 3/5 fragmentation of the andesite sample. The fragmentation speed was calculated to be in the range of 7.8 to 12.2 m/s. At a ΔP of 25 MPa the lower transducer shows two kinks. We interpret the first kink as full fragmentation (30.6 m/s) and the second one as resulting from a particle that tried to rotate in the trajectory, blocking the autoclave and thus led to a reduced decompression speed. At the instant when either by fragmentation or further rotation the particle was removed, the second kink results, marking the higher gas decompression rate.

the 1995 eruption of Unzen (Japan); (2) three basaltic andesite samples from the 1994 eruption of Merapi (Indonesia); and (3) the grey dacite representing the cryptodome material of the 18 May 1980 eruption of Mount St. Helens.

The youngest eruption of the Unzen volcano complex occurred at the summit of Fugendake. It started in 1990 and lasted until 1995, producing mainly Merapi-type block-and-ash flows due to the gravitational collapse of the growing domes (Nakada et al., 1999). The investigation of a sample with an open porosity of 21.5 vol% (sample MUZD Ui) resulted in a fragmentation threshold of 8.1–10.3 MPa at 20°C, whereas the threshold was exceeded at 3–3.5 MPa with an elevated temperature of 900°C. For a sample with $\sim$16.4 vol% open porosity (sample FD24693) the predetermined fragmentation threshold at 20°C is $\sim$6 MPa (Spieler, 2001). By raising the temperature to 900°C this value is reduced to $\sim$3.5 MPa. The threshold of a sample with 9 vol% porosity (sample ENSP) at 20°C is $\sim$8 MPa. The starting materials contain broken phenocrysts where the crystal fragments are nevertheless still in the original orientation, i.e. the cracks have not opened apart significantly.

The block-and-ash flows of Merapi type eruptions are triggered by steady magma injection into the dome leading to instability and lateral dome collapse (Voight and Elsworth, 2000). As noted above for Unzen, most phenocrysts in the trachytic groundmass of the basaltic andesite of Merapi are broken but intact. The open porosity of the material found in the pyroclastic flows of Merapi's 1994 eruption covers a range of 5–65 vol% and exhibits a wide textural variety.

The fragmentation threshold of highly porous samples ($>$50 vol% vesicularity) with vesicles connected to crystal surfaces and 25–30 vol% crystal content is as low as 2.5 MPa (Spieler, 2001). Below a porosity of 50 vol% the vesicle–form parameters (2-D vesicle area vs. length of the outline and shape) change, from an interconnected irregular network into a short range net-

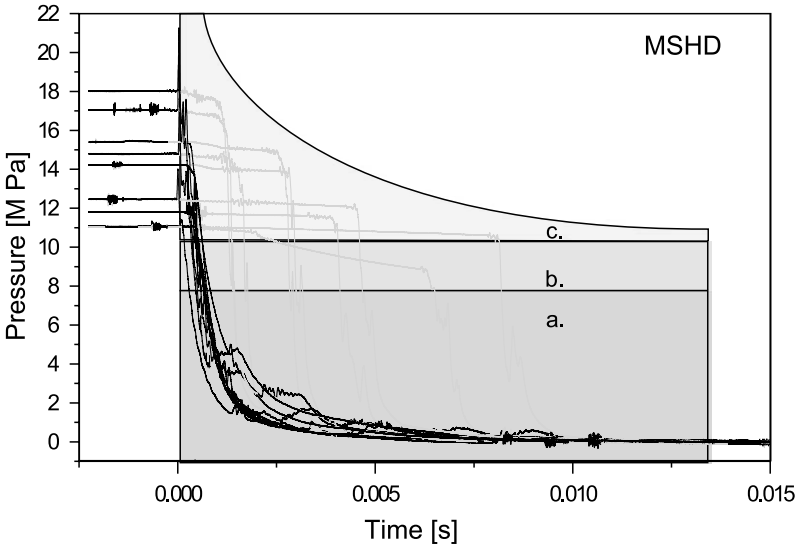

Fig. 7. Results of nine dynamic fragmentation experiments on Mount St. Helens grey dacite. The increase in pressure from 11 to 18 MPa leads to an increase of the fragmentation front velocity from 6.5 to 54 m/s, respectively. Three reaction fields can be distinguished: (a) the permeability controlled gas flow regime (where the gas pressure is reduced due permeable gas flow through connected porosity and cracks), (b) decompression controlled fragmentation threshold (the beginning of the pressure controlled fragmentation depends on density variations in the natural samples), and (c) the pressure controlled fragmentation. In (c) a clear increase of the fragmentation velocity with raising ΔP_{fr} is seen (full fragmentation of the sample).

work of a few spherical vesicles and the connectivity of vesicles to crystal surfaces is drastically reduced. The initial pressure difference controlling the fragmentation threshold rises to 8 MPa and for samples with 5–10-vol% vesicles to >15 MPa. In the present study we focus on a sample with 59.8 vol% open porosity (sample MRP 9603) that provided the highest fragmentation wave velocity and an unusually strong material sample MRP9606 with $\sim$25.3 vol% open porosity (Fig. 9).

Mount St. Helens grey dacite (sample MSHD) has been studied in detail in previous fragmentation experiments (Alidibirov and Dingwell, 1996a; Spieler et al., 2003). The material has a microporous groundmass with an highly interconnected open porosity of $\sim$36% and a phenocryst content of 30%. The phenocrysts are broken and the fragments are separated by voids. A fragmentation threshold of 9 MPa was determined for this cryptodome dacite at room temperature. This value was reduced to 3 MPa at 900°C. The records of 9 experiments above the threshold of 9 MPa are shown in Fig. 7.

4. Fragmentation speed results

A series of room temperature experiments has been performed at initial pressure difference (ΔP) values ranging from well below the fragmentation threshold to values above the threshold pressure (ΔP_{fr}). (In this investigation ΔP_{fr} is defined as the pressure difference that produced the first fragmentation of the sample cylinder.) In Figs. 4–7 sets of dynamic pressure traces obtained from the transducers above and below the samples are plotted. Each experiment is represented by a pair of lines corresponding to the upper (black) and lower (grey) pressure transducers. Opening of the diaphragm triggers the RW travelling at $\sim$340 m/s into the autoclave. The arrival of the RW at the upper (free) sample surface is recorded by the first pressure transducer (P1).

The highest pressure difference is experienced by the sample when the RW intersects the porous sample surface. At depth in the sample, sample permeability may allow for significant gas filtration leading to a reduced pressure difference (ΔP_{red}) and the development of a smoothed RW

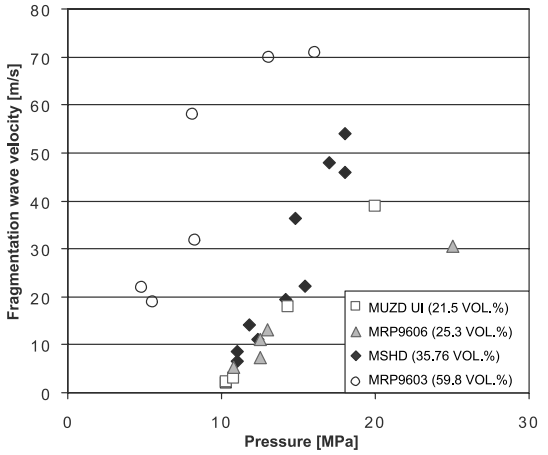

Fig. 8. The influence of porosity on the velocity of the fragmentation wave is shown by the results of 25 experiments (Table 1). Sample MRP9603 with a porosity of 59.8 vol% resulted in the highest velocities and lowest threshold. A comparision of MSHD with 35.76 vol% and MUZD UI (21.5 vol%) shows slightly elevated values for the 14.26-vol% higher MSHD only. The reversed case is given for the nearly identical MRP9606 (25.3 vol%) experiment. Here the fragmentation speed is lower. MRP 9606 had an unusually high threshold at 900°C (Fig. 9).

for the sample interior. Thus the actual threshold (in the natural system) might be slightly higher than the reported, since the expansion energy stored in the gas phase has to be proportional to the initial ΔP leading to a fragmentation (ΔP_{fr}). The condition $\Delta P_{red} \geq \Delta P_{fr}$ must be satisfied for a self-sustained fragmentation process. If no fragmentation occurs, the pressure below the sample decreases at a rate controlled by the permeability of the sample. Provided the permeability does not increase due to the removal of a part of the sample or internal fracturing, the same decompression rate is recorded below the sample. This is the case when permeability is controlled by short range connectivity as well as in the case of a predominance of closed pores.

When the decompression is recorded at the surface of the sample, the pressure line of the first transducer (P1) drops rapidly below 0.2 MPa. In contrast, the pressure below the sample decreases initially relatively slowly. If the sample fragments, then the initially slow decompression recorded by the lower pressure transducer (P2) yields to a rapid pressure drop signalling the loss of the sample due to fragmentation. Repetition of 'no-fragmentation' or 'sub-fragmentation' experiments (those for which fragmentation does not occur because the fragmentation threshold was not reached) on samples where only 1–5 mm were removed by a previous experiment did not lead to progressively changed (faster) decompression behaviour below the sample, even at pressures only slightly (0.5–1 MPa) below ΔP_{fr} (Figs. 4 and 6).

For the case of sample fragmentation the time between the recorded pressure drop at P1 (t_1) and the pressure drop at P2 (t_2) corresponds to the time interval T_{fr} the duration of the fragmentation of the magma. T_{fr} in combination with the sample length is then used to calculate the fragmentation speed (Figs. 4–7). The fragmentation speed is defined as $N = L/T_{fr}$, where $L = 50$ mm (length of fragmentation), $T_{fr} = t2 - t1$ (duration of fragmentation).

Fig. 4 illustrates the pressure history of six experiments on a dacite from Unzen with 16.4 vol% open porosity (FD24693). Each experiment is represented by a pair of recorded pressure signals (P1 and P2). In the first two experiments at 2.8 and 3.2 MPa, respectively, i.e. far below the ΔP_{fr} of 8–8.5 MPa, no fragmentation occurred. The pressure path of P1 (black) shows the characteristic rapid pressure drop above the sample surface. P2

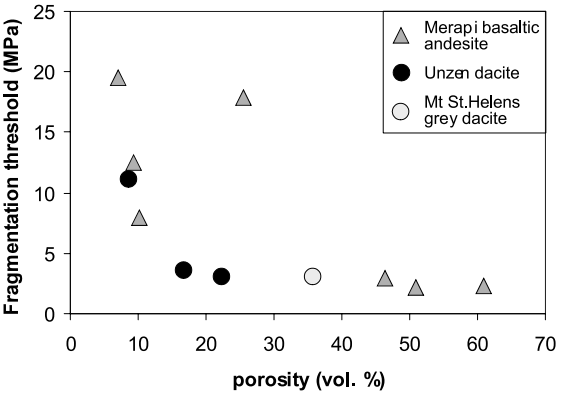

Fig. 9. The fragmentation threshold vs. porosity (experiments at 900°C) plot demonstrates the strong influence of porosity on fragmentation. The values derive from experiments on Merapi basaltic andesite (triangles), Mount St. Helens grey dacite (grey circle) and Unzen dacite (black circles). The data point at 17 MPa and 25.3 vol% corresponds to MRP9606, an unusually strong material (compare Fig. 8).

(grey), at the second transducer, gives the characteristic permeability-controlled slow decompression. ΔP was raised to 4 MPa in the third experiment. Again the rapid decompression is recorded at P1 and the slow permeability below the sample. The fourth experiment was performed at 7.4 MPa (close to the ΔP_{fr} of 8–8.5 MPa) producing the same characteristics of a no-fragmentation experiment. At 8.6 MPa a sudden pressure drop was recorded below the sample and interpreted as the first fragmentation. Thus the fragmentation threshold (at 20°C) is in the pressure range of 7.5–8.5 MPa.

To analyse whether the sub-ΔP_{fr} experiment (performed at pressures slightly below the threshold) changed the permeability we reduced ΔP_0 to 5.7 MPa. The change of the permeability should lead to an increased decompression rate below the sample (steeper drop of the P2 line). If the trace of P2 falls directly between the P2 records of the previous two experiments no evidence for the onset of the rapid filtration flow must be inferred. The recorded data do indeed plot directly between the previous lines proving that no fragmentation occurred due to the mechanism of the rapid filtration flow (Alidibirov and Dingwell, 2000). An elevated $\Delta P_0 = 8.5$ MPa produced a fragmentation of the sample. In all 30 mm of the sample were removed and ejected into the LPT. The P2 record exhibits a short permeability controlled degassing period of 6.16 ms until the degassing history shows a rapid pressure drop. The modification due to the fragmentation of 60% of the sample proves the important role of the short-range connectivity of pores. The speed of the fragmentation N at ΔP_{fr} was calculated for 30 mm and 50 mm lengths, respectively, and a duration of 6.16 ms to be $N_{30\,mm} = 4.9$ m/s and $N_{50\,mm} = 8.1$ m/s. The $N_{50\,mm}$ calculation was performed to demonstrate the possible range of such an experiment since the pressure information had to path from the new surface to the transducer and the delay is not known. Here we recognise the dependence of ΔP and the effective decompression rate $|dP/dt|_{fr} = \Delta P_{fr}/t_1$ on the physical properties of the sample.

The investigation of the fragmentation speed of Merapi andesite was performed on two samples (MRP9606, MRP9603) with ~25.3 vol% open porosity (close to the previous dacite of Unzen) and 59.8 vol%, respectively (Table 1). Fig. 6 illustrates the data recorded in five experiments on MRP9606 at $\Delta P_0 = 7.3$, 9.3, 11.5, 12.5, and 25 MPa, respectively (where $\Delta P_0 = 12.5$ MPa corresponds to ΔP_{fr}). As discussed already, the decompression below the sample (P2) is controlled by the permeability of the sample (i.e. the connectivity of pores). The texture of the pores as well as the crystal size and content (size of crystal fragments) differs from the Unzen dacite. The pores are attached to the crystal surfaces. In Fig. 6, the three experiments below ΔP_{fr} demonstrate a high permeability in comparison to Fig. 5 (MUZD Ui with 21.5 vol%). This, in turn, generates a higher ΔP_{fr}. The fragmentation velocity N calculated from the experiment at ΔP_{fr}, calculated for 32 mm and 50 mm length respectively and a duration of 4.3 ms, is $N_{32\,mm} = 7.4$ m/s and $N_{50\,mm} = 11.6$ m/s. The major physical difference between the samples is the vesicle texture (free surface) and distribution and the degree of the phenocryst shattering present in these natural samples.

Using a 0.5-mm graphite rod a speed of ~40 m/s was recorded at 900°C and 12 MPa. This fragmentation speed is four times higher than those observed at room temperature and is thus a clear indication that high-temperature experiments are needed for comparison to natural eruptive conditions.

These experimental results yield five fundamental observations:

Firstly, the fragmentation speeds are low and found typically to be two to three orders of magnitude smaller than the speed of sound which may serve as an upper limiting value. In the present study, fragmentation velocities as low as ~2 m/s (Fig. 5; Table 1) have been obtained for a dacite sample with 21.5 vol% open porosity from Unzen (MUZD UI) at a pressure of 10 MPa, close to the ΔP_{fr}. Raising the ΔP_0 by 1 MPa to 11 MPa resulted in a fragmentation velocity of 3 m/s, or 42% faster. We conclude that the fragmentation velocity N increases with the increase of ΔP_0 (Fig. 8) as well as with the resulting increase of the effective decompression rate $|dP/dt|_{fr} = \Delta P_{fr}/t_1$.

Secondly, our experiments reveal that the differ-

Table 1
Conditions and results of fragmentation speed determinations

Sample	Density calculated	Density accupyc	Porosity open (%)	Porosity closed (%)	Initial pressure difference (ΔP) (MPa)	Fragmentation speed (m/s)
MSHD	1.51	2.34	35.76	6.4	11.0	(*2 experiments*) 6.5–8.6
					11.8	14.2
					12.4	11.2
					14.2	19.5
					14.8	36.3
					15.4	22.2
					17.0	48
					18.0	46–54
MSHD (900°C)	1.51	2.34	35.76	6.4	12.0	40
MUZD Ui	1.84	2.33	21.5	5.6	4.6	no frag.
					7.8	no frag.
					10.3	1.9–2.3
					10.8	3.0
					14.3	18.0
					20.0	38.9
ENSP	2.37	2.6	8.71	<1	4.7	no frag.
					5.1	no frag.
					5.4	no frag.
					6.6	no frag.
					8.1	no frag.
					8.9	no frag.
					9.8	no frag.
					11.0	(partial frag.)
					11.4	12.2
					12.0	(partial frag.)
FD24693	2	2.57	16.4	<4	3.0	no frag.
					3.2	no frag.
					4.0	no frag.
					5.6	no frag.
					7.4	no frag.
					8.6	4.9–8.1
					11.3	19.6
MRP 9603	1.13	2.82	59.84	0.51	2.6	no frag.
					3.3	no frag.
					4.5	no frag.
					4.8	21.9
					5.5	18.7–19.2
					8.1	58
					8.3	31.85
					11.5	31.58
					13.1	69.88
					16.1	71
MRP 9606	2.07	2.77	25.3	0.3	2.7	no frag.
					3.1	no frag.
					4.6	no frag.
					4.7	no frag.
					8.5	no frag.
					9.5	no frag.
					10.0	no frag.
					10.8	<5.2 (partial frag.)
					11.5	1 mm removed
					12.5	7.4–11.2
					13.0	13.2
					25.0	18.2–30.6

ential pressure $\Delta P_{fr} = P_{fr} - P_0$ (P_0 = pressure in the LPT) at which the experimental fragmentation of a magma occurs is a critical parameter controlling the fragmentation onset itself (Fig. 9). We emphasise that this parameter is likely to be slightly below the value of the differential that is responsible for the case of a self-sustained eruption in nature. Thus although we determine ΔP_{fr}, a self-sustained eruption may require that $\Delta P_0 > \Delta P_{fr}$.

Thirdly, higher magma porosity yields higher fragmentation speeds (Fig. 8). In a dacite sample with 16.4 vol% of open porosity, the fragmentation speed, (N), reaches a velocity of 8.1 m/s slightly above the threshold pressure of 8.5 MPa (Fig. 4). The higher porosity may influence the strength in several ways. Larger vesicles may yield a higher specific free surface, a higher connectivity (this should influence the ΔP inside the sample (ΔP_{red}) due to permeable gas flow) and a reduced vesicle wall thickness leading to a weaker structure. With an increase of the gas volume, the internal energy stored in the gas phase increases. Larger vesicles may influence the thickness and velocity of the fragmentation front as a larger distance can be obtained by opening a single layer of vesicles.

Fourthly, preliminary high-temperature experiments yield fragmentation speeds consistent with those obtained at low-temperature, implying that the experimental results and their systematics obtained here are applicable to magmatic temperatures.

Finally, an additional observation, of potential importance for the eruption dynamics is that although low-porosity material (Sample MRP9618, 7% porosity) was fragmented at $\Delta P_{fr} > 18$ MPa, the transport energy of the expanding gas was too small to eject the total sample into the LPT.

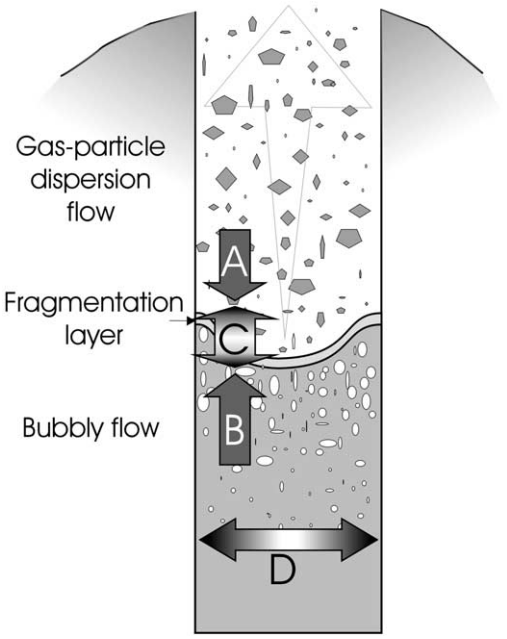

Fig. 10. A 1-D conceptual sketch of the dynamics surrounding the depth of the fragmentation front. The depth to the fragmentation front may be a delicate interplay between the speed of fragmentation (A) and the ascent speed (B). An imbalance in these two speeds may lead to a fragmentation front which either rises or drops with time (C). Unsteady conditions may be the rule where drops and rises in the fragmentation depth follow each other. A perfectly steady depth to fragmentation may be possible during long-lived eruptions where the balance of ascent and fragmentation speeds is met. Density changes over the diameter of the conduit (D) will influence the spatial position of the fragmentation front and affect the local pressure situation.

5. Discussion

The pressure histories recorded as well as the particles gained in the present study suggest that the fragmentation occurs in planes perpendicular to the decompression axis of the samples. The fragmentation speed of porous magma in the range of 9–60 vol% correlates positively with porosity. The speed recorded at pressure differences near the fragmentation threshold is as slow as 2.1 m/s. The upper limit of the decompression wave velocity is the speed of sound in the pressurised foam (up to $\sim$3400 m/s), for the fragmentation wave the expansion of the gas phase is considered to be the maximum velocity.

The slow speed (< 5 m/s) and the high pressure (> 16 MPa) of fragmentation for low-porosity magma will influence the dynamics and evolution of the eruption column. The application of the experimentally derived fragmentation speeds to numerical models may lead to a better understanding of the dynamic situation at the fragmen-

tation. A density and pressure dependent velocity of the fragmentation front whose dynamics balances the ascent speed of the magma column will generate a steady state eruption (Fig. 10). Perhaps an unsteady position of the fragmentation front is the more general case where the balance between ascent velocity and fragmentation front speed switches back and forth between regimes of ascending and descending fragmentation front depth. Further influence on the propagation and spatial location of the fragmentation front may be provided by density changes from the wall to the centre of the conduit. Finally, we speculate that the high-pressure, low-porosity fragmentation will, in contrast, lead to the collapse of the column feed and cessation of the explosive eruption.

6. Conclusion

The experimental data presented herein demonstrate the strong influence of porosity on the fragmentation threshold of natural magmatic samples. Our experimental results confirm an early hypothesis, based mainly on studies of textures of natural pyroclasts (McBirney and Murase, 1970; Bennett, 1974; Heiken and Wohletz, 1985, 1991), and later placed on a mechanistic basis (Dingwell and Webb, 1989, 1990) that the disruption of magma can be accomplished by the application of tensile stresses in a brittle response regime. Further it has been demonstrated that the increase of the effective decompression rate leads to an increase of the fragmentation wave velocity.

Acknowledgements

We acknowledge the financial support by the Deutsche Forschungsgemeinschaft (Di-431). We wish to thank all the people and institutions involved in the Merapi project. We are grateful to R. Hoblitt and C.D. Miller for providing samples of Mount St. Helens dacite. Thanks are due also to T. Ui, S. Nakada, H. Shimizu, and the staff of the Shimabara Volcano Observatory for their kind help on Unzen. The reviewers M. Ichihara, O. Melnik and R. Mason helped to improve the paper.

References

Alidibirov, M.A., 1994. A model for viscous magma fragmentation during volcanic blasts. Bull. Volcanol. 56, 459–465.

Alidibirov, M., Dingwell, D.B., 1996a. Magma fragmentation by rapid decompression. Nature 380, 146–148.

Alidibirov, M., Dingwell, D.B., 1996b. An experimental facility for investigation of magma fragmentation by rapid decompression. Bull. Volcanol. 58, 411–416.

Alidibirov, M., Dingwell, D.B., 2000. Three fragmentation mechanisms for highly viscous magma under rapid decompression. J. Volcanol. Geotherm. Res. 100, 413–421.

Barclay, J., Riley, D., Sparks, R.S.J., 1995. Analytical models for bubble growth during decompression of high viscosity magmas. Bull. Volcanol. 57, 422–431.

Bennett, F.D., 1974. On volcanic ash formation. Am. J. Sci. 274, 648–661.

Cashman, K.V., Mangan, M.T., 1994. Physical aspects of magma degassing, II. Constraints on vesiculation processes from textural studies of eruptive products. In: Carroll, M.R., Holloway (Eds.), Volatiles in Magmas. Mineral. Soc. Am., Washington, DC, pp. 446–478.

Dingwell, D.B., Webb, S.L., 1989. Structural relaxation in silicate melts and non-Newtonian melt rheology in igneous processes. Phys. Chem. Miner. 16, 508–516.

Dingwell, D.B., Webb, S.L., 1990. Relaxation in silicate melts. Eur. J. Mineral. 2, 427–449.

Dingwell, D.B., 1998a. Recent experimental progress in the physical description of silicic magma relevant to explosive volcanism. In: Gilbert, J.S., Sparks, R.S.J. (Eds.), The Physics of Explosive Volcanic Eruptions. Geol. Soc. Lond. Spec. Publ. 145, pp. 9–26.

Dingwell, D.B., 1998b. In: Freund, A., Rosi, M. (Eds.), From Magma to Tephra: Modelling Physical Processes of Explosive Volcanic Eruptions. Developments in Volcanology. Elsevier, Amsterdam, pp. 1–24.

Fink, J., Kieffer, S.W., 1993. Estimate of pyroclastic flow velocities resulting from explosive decompression of lava domes. Nature 363, 612–615.

Heiken, G.H., Wohletz, K.H., 1991. Fragmentation processes in explosive volcanic eruptions. In: Sedimentation in Volcanic Settings. SEPM Spec. Publ. 45, pp. 19–26.

Hill, L.G., Sturtevant, B., 1990. An experimental study of evaporation waves in superheated liquid, in Adiabatic Waves in Liquid-Vapor Systems. Meier, G.E.A., Thompson, P.A. (Eds), IUTAM Symposium Göttingen, 1989, pp. 25–37.

Hurwitz, S., Navon, O., 1994. Bubble nucleation in rhyolitic melts: Experiments at high pressure, temperature, and water content. Earth Planet. Sci. Lett. 122, 267–280.

Ichihara, M., Rittel, D., Sturtevant, B. (2002) Fragmentation

of a porous viscoelastic material: Implications to magma fragmentation. J. Geophys. Res., 107-B10, 10.1029/2001JB000591.

Kaminski, E., Jaupart, C., 1998. The size distribution of pyroclasts and the fragmentation sequence in explosive volcanic eruptions. J. Geophys. Res. 103, 29759–29779.

Mader, H.M., Zhang, Y., Phillips, J.C., Sparks, R.S.J., Sturtevant, B., Stolper, E., 1994. Experimental simulations of explosive degassing of magma. Nature 372, 85–88.

Mader, H.M., Phillips, J.C., Sparks, R.S.J., Sturtevant, B., 1996. Dynamics of explosive degassing of magma: Observations of fragmenting two-phase flow. J. Geophys. Res. 101, 5547–5560.

Martel, C., Dingwell, D.B., Spieler, O., Pichavant, M., Wilke, M., 2001. Experimental fragmentation of crystal- and vesicle-bearing silicic melts. Bull. Volcanol. 63, 398–405.

Martel, C., Dingwell, D.B., Spieler, O., Pichavant, M., Wilke, M., 2000. Foaming and fragmentation in silicic melts: An experimental study. Earth Planet. Sci. Lett. 178, 47–58.

McBirney, A.R., Murase, T., 1970. Factors governing the formation of pyroclastic rocks. Bull. Volcanol. 34, 372–384.

Melnik, O.E., 2000. Dynamics of two-phase conduit flow of high-viscosity gas-saturated magma: Large variations of sustained explosive eruption intensity. Bull. Volcanol. 62, 153–170.

Nakada, S., Shimizu, H., Ohta, K., 1999. Overview of the 1990–1995 eruption at Unzen volcano. J. Volcanol. Geotherm. Res. 89, 1–22.

Papale, P., 1999. Strain-induced magma fragmentation in explosive eruptions. Nature 397, 425–428.

Phillips, J.C., Lane, S.J., Lejeune, A.-M., Hilton, M., 1995. Gum-rosin-aceton system as an analogue to the degassing behaviour of hydrated magmas. Bull. Volcanol. 57, 263–268.

Proussevitch, A.A., Sahagian, D.L., Anderson, A.T., 1993. Dynamics of diffusive bubble growth in magmas: Isothermal case. J. Geophys. Res. 98, 22283–22308.

Proussevitch, A.A., Sahagian, D.L., 1998. Dynamics and energetics of bubble growth in magmas: Analytical formulation and numerical modelling. J. Geophys. Res. 103, 18223–18251.

Sato, H., Fujii, T., Nakada, S., 1992. Crumbling of dacite dome lava and generation of pyroclastic flows at Unzen volcano. Nature 360, 664–666.

Sparks, R.S.J., 1978. The dynamics of bubble formation and growth in magmas: A review and analysis. J. Volcanol. Geotherm. Res. 28, 257–274.

Sparks, R.S.J., Barclay, J., Jaupart, C., Mader, H.M., Phillips, J.C., 1994. Physical aspects of magma degassing, I. Experimental and theoretical constraints on vesiculation. Rev. Mineral. 30, 414–445.

Spieler, O., 2001. Die Fragmentierung hochviskoser Magmen: Experimenteller Aufbau und Analysetechniken. Ph.D. Thesis, LMU München (urn = nbn:de:bvb:19–4303).

Spieler, O., Alidibirov, M., Dingwell, D.B., 2003. Grain-size characteristics of experimental pyroclasts of 1980 Mount St. Helens cryptodome dacite Effects of pressure drop and temperature. Bull. Volcanol. 68, 90–104.

Sugioka, I., Bursik, M., 1995. Explosive fragmentation of erupting magma. Nature 373, 689–692.

Thomas, N., Jaupart, C., Vergniolle, S., 1994. On the vesicularity of pumice. J. Geophys. Res. 99, 15633–15644.

Voight, B., Elsworth, D., 2000. Instability and collapse of hazardous gas-pressurized lava domes. Geophys. Res. Lett. 27, 1–4.

Wohletz, K.H., McQueen, R.G., 1984. Experimental studies of hydro-magmatic volcanism. In: Studies in Geophysics. Explosive Volcanism: Inception, Evolution, and Hazards. Academic Press, Washington, DC, pp. 158–169.

Zhang, Y., Sturtevant, B., Stolper, E.M., 1997. Dynamics of gas-driven eruptions: experimental simulations using CO_2–H_2O–polymer system. J. Geophys. Res. 102, 3077–3096.

Zhang, Y., 1999. A criterion for the fragmentation of bubbly magma based on brittle failure theory. Nature 402, 648–650.

Zimanowski, B., Büttner, R., Lorenz, V., Häfele, H.-G., 1997. Fragmentation of basaltic melt in the course of explosive volcanism. J. Geophys. Res. 102, 803–814.